Research Article

Israel Journal of Chemistry
www.ijc.wiley-vch.de

doi.org/10.1002/ijch.202300005

Mixed Germania-Silica Films on Ru(0001): A Combined Experimental and Theoretical Study

Alexander Fuhrich,[a] Joachim Paier,[a] Sergio Tosoni,[b] Adrián Leandro Lewandowski,[a] Leonard Gura,[a] Wolf-Dieter Schneider,[a] Gianfranco Pacchioni,[b] and Hans-Joachim Freund*[a]

Dedicated to Helmut Schwarz on the occasion of his 80th birthday.

Abstract: Two-dimensional oxide films are potentially useful for future technological applications, but also important objects to study model catalyst systems on the more fundamental side. Here we study silica, germania, and mixed silica-germania films supported on a metal single crystal surface Ru(0001). Those mixed films are interesting objects to systematically modify the properties of silica films, which may be used as membranes or covers for model studies in confined space, due to the modification of the rather stiff silica layers by incorporating germanium atoms replacing silicon atoms. Here we report a combined experimental and theoretical study of such layers, where we show how X-ray photoelectron spectroscopy in combination with LEED and I/V LEEM measurements allow us to judge the formation of such mixed films.

Introduction

Two-dimensional films have a high potential for manifold technological applications. Consequently, they have stimulated a very intense research activity in the past and are, at present, still at the forefront of condensed matter investigations. Two-dimensional systems range from single elements, like graphene, to complex heterostructures.[1] In addition to transition metal dichalcogenides (TMDs), which show promising properties for spin-polarized currents,[2] oxides are being investigated due to their versatile properties, e.g., in electronics and in catalysis.[3]

Specifically, silica is used as a support material for catalytically active materials. Moreover, two-dimensional silica films may be hydroxylated.[4] Modified two-dimensional silica films are very suitable model systems for catalysts, due to their reduced complexity compared to powder-based catalysts. As these model systems are accessible to a variety of surface-science characterization methods and theoretical calculations, fundamental processes in catalysis can be studied at the atomic level.[5]

Silicon dioxide (SiO_2, silica) exists in a large number of different structures in the bulk.[6] For 2D silica bilayers (BL), crystalline and vitreous structures are dominant. In addition, a metastable two-dimensional zig-zag structure has been identified which transforms into a stable 2D silica BL structure upon annealing at high temperature.[7] In 1932 Zachariasen proposed an atomic network structure model for a 2D glass.[8] This model was experimentally confirmed for 2D crystalline and vitreous silica (BL) on Ru(0001) using atomically resolved scanning tunneling and atomic force microscopy images (STM and AFM).[9] A detailed review of two dimensional silica films and their modifications can be found in Ref. [10]. Recently, in addition to the preparation of silica on metal single crystals using electron beam evaporators, two-dimensional silica films have been successfully prepared by self-limiting atomic layer deposition (ALD) on metal foils.[11] This achievement most probably will lead to important applications in large scale thin film technology.

The two-dimensional silica films are bound to the metal support via weak van der Waals bonds. Nevertheless, the nature of the substrate has a significant influence on the two-dimensional film growth and on the electronic structure of the film. For example, antimonene, the two-dimensional modification of antimony, is transformed from an indirect to a direct semiconductor on Cu_3O_2, due to stress induced by the lattice mismatch between substrate and film.[12] In 2D silica films, the choice of the metallic support determines the structure of the film.[13] On Mo(112) only the crystalline monolayer (ML) is observed, while on Ru(0001) the ML and BL are formed. On the latter substrate the BL can be vitreous or crystalline, or even a mixture of both phases. On less oxygen-affine

[a] *A. Fuhrich, J. Paier, A. Leandro Lewandowski, L. Gura, W.-D. Schneider, H.-J. Freund*
Fritz Haber Institute of the Max Planck Society
14195 Berlin, Germany
E-mail: freund@fhi-berlin.mpg.de
[b] *S. Tosoni, G. Pacchioni*
Accademia Nazionale dei Lincei, Universita' degli Studi di Milano-Bicocca, Dipartimento di Scienza dei Materiali
20125 Milano, Italy

Supporting information for this article is available on the WWW under https://doi.org/10.1002/ijch.202300005

substrates, such as Pt(111), the vitreous BL is formed,[13] on Au(111) the crystalline BL has been observed.[14]

In the periodic table germanium is located below silicon and accordingly has similar chemical and physical properties. Germania forms glasses similar to silica. In contrast to silica, germania is catalytically active by itself, and can be used as a catalyst for PET(Polyethylene-terephthalat) production.[15] Ge-doped silica or mixed GeO_2–SiO_2 glasses find important applications in the field of optical fibers,[16] nanoscale modification of optical properties in Ge-doped SiO_2 glass by electron-beam irradiation, anode materials for Lithium-ion batteries[17] or memristors.[18]

The growth properties of germania films on different metallic substrates follow a trend already observed for silica. On Ru(0001) only a germania ML is formed, on Pt(111) both the ML and BL exist in crystalline and vitreous form.[12–13,19] Consequently, the Pt(111) support for germania is comparable to the Ru(0001) support for silica.[13] Germania only forms the vitreous BL structure on Au(111),[20] which is also the case for the silica film on Pt(111).[13]

Mixed 2D germania-silica films are of considerable interest as model systems for heterogeneous catalysis. In their vitreous phases they exhibit large Si–O and Ge–O ring sizes[9,13,21] and consequently mimic in two dimensions the trends towards mesoporous zeolite structures found in synthesized 3D germanosilicates.[22] Therefore, the investigation of mixtures of both oxides on a metal support presents a worthwhile challenge for experiment and theory[23] to model germanium substituted alumina-zeolites. In the present work, the atomic and electronic structure of different mixed germania-silica films on a Ru(0001) support has been elucidated by a combined effort of spectro-microscopy and density functional theory (DFT). Cohesive energies, atomic structure and stability, lattice parameters for free standing silica, germania, and mixed silica-germania BL, adhesion energies on the Ru support, DOS of the films on the Ru-support as well as work function changes of the combined film substrate-system have been calculated and are compared with the corresponding experimental results (see SI). An interesting observation concerns the influence of the detailed preparation method of the silica-germania films. If Ge is deposited in oxygen atmosphere on top of an ordered silica film, the XPS 3d core level spectra show that the resulting germania film desorbs completely from the silica film upon annealing to 970 K. However, if Ge is deposited in oxygen atmosphere on a disordered silica film, the persisting presence of the Ge-3d core level signal at 970 K indicates that a mixed phase of a silica-germania film has been obtained.

Experimental Details

The experiments were performed using the LEEM/XPEEM (Low Energy Electron Microscopy/X-Ray Photoemission Electron Microscopy) microscope SMART (Spectro-Microscopy with Aberration correction for Relevant Techniques) located at the UE49-PGM beam line of the synchrotron light source BESSY II of the Helmholtz Center Berlin (HZB).[24] The SMART microscope combines low-energy electron microscopy and diffraction techniques (LEEM, LEED (Low Energy Electron Diffraction)) with spectroscopic techniques (XPEEM, XPS (X-ray Photoelectron Spectroscopy), VB (Valence Band) mapping) and operates at a base pressure of 10^{-10} mbar. The SMART microscope compensates the spherical aberration and chromatic aberration and has a lateral resolution of 2.6 nm in LEEM and 18 nm in XPEEM. The worse lateral resolution is caused by space charge effects in XPEEM due to the pulsed light structure of the synchrotron light. The energy resolution of the Omega electron energy filter is 180 meV. The XPS measurements were performed at room temperature in UHV. The photon energies were chosen so that the resulting kinetic energy of the photoelectrons is about 70 eV, which is very surface sensitive. The intensities of the photoelectron spectra were normalized to the background intensities for comparison.

The sample temperature was measured by a thermocouple (W26%Re/W5%Re) spot-welded to the sample holder at the backside of the sample. In addition, a pyrometer (Lumascence Technologies, IMPAC IGA 740) with an absolute accuracy of about 10 K is available. Oxygen (99.999% purity) was dosed by a leak valve directly into the main chamber.

The Ru(0001) crystal has a miscut below 0.2°. The ruthenium crystal was cleaned by several Ar^+ sputtering and annealing cycles, based on the cleaning steps suggested in Ref. [25]. The Ar^+ sputtering was performed with an ion energy of 1.5 kV for 10 min with a current of 1 μA. The first annealing step after sputtering was done in $1*10^{-6}$ mbar O_2 for 10 min at 1170 K. Subsequently, the sample was annealed for 10 min in UHV at 1420 K. Finally, the ruthenium sample was flashed in UHV for one minute at 1520 K. In LEEM the surface appears smooth and clean. The Ru(0001) surface has a high affinity to oxygen[26] and forms well-ordered adsorbate structures with oxygen, e.g., the 3O-(2×2)-Ru(0001) surface.[27] Oxygen chemisorbs on the hcp hollow sites on Ru(0001). The 3O-(2×2)-Ru(0001) was prepared by annealing the Ru(0001) crystal in oxygen atmosphere ($1*10^{-6}$ mbar O_2 for 10 min at 1170 K). In the present work only the 3O-(2×2)-Ru(0001) and the bare Ru(0001) surface were used for the subsequent depositions of Si and Ge. A detailed overview of the properties for the Ru(0001) substrate and O-adlayers in relation to the preparation of ultra-thin silica films can be found in Refs. [28]. The preparation of ultrathin silica films on various substrates is well known.[10] Silicon and germanium (Alfa powder 100 mesh purity 99.999%) were evaporated by a commercial Focus GmbH EFM3 UHV evaporator with ion suppressor, which points towards the sample in measurement position under a grazing angle of 20°.

Different annealing temperatures and oxygen pressures can be used to produce crystalline or vitreous SiO_2 films on Ru(0001). The amount of Si applied determines whether a silica ML or BL is formed. If there is an excess amount of Si in a BL, the excess amount desorbs during annealing. The

calibration of the Si amount was done according to Ref. [28b]. A germania ML can be prepared on Ru(0001).[13,19,29]

Mixed GeO_2–SiO_2 films were prepared by sequential physical vapor deposition of Ge on (i) disordered SiO_x and (ii) on ordered SiO_2. In the cases studied here, a SiO_2 fraction of 1.5 ML and a GeO_2 fraction of 0.5 ML were chosen. Other mixing ratios are possible. The preparation recipes for the two different types (i) and (ii) of mixed Germania-Silica films consist of the following steps. (i) First, silicon is deposited on 3O-(2×2)-Ru(0001) in $2*10^{-7}$ mbar O_2 atmosphere at RT. This step is similar to the standard preparation method for silica films on Ru(0001). A detailed description can be found in Refs. [28b,30]. Next, germanium is deposited in $2*10^{-7}$ mbar O_2 atmosphere at 570 K on top of the disordered SiO_x film. Finally, the sample is annealed to 720 K and to 970 K for 10 min in in $1*10^{-6}$ mbar O_2. (ii) Ordered (2×2) SiO_2 films were prepared by annealing the SiO_x film to 1050 K in $1*10^{-6}$ mbar O_2. Subsequently, germanium is deposited onto this silica film in $2*10^{-7}$ mbar O_2 at room temperature. A final annealing of the film to 720 K and to 970 K for 10 min in in $1*10^{-6}$ mbar O_2 terminates the sample preparation.

Computational Details

Periodic DFT calculations were performed with the VASP (Vienna Ab initio Simulation Package) program.[31] The PBE (Perdew-Burke-Ernzerhof)[32] exchange-correlation functional was used in all calculations. To optimize the lattice parameter of the perfect hexagonal bilayer unit cells, a Γ-centered k-point mesh in the Monkhorst-Pack[33] scheme was used which was set to (5×5×1). The kinetic energy cutoff for the expansion of the plane wave basis set was set to 400 eV. All slabs were separated by more than 12 Å of vacuum, and we included dipole corrections.[34]

Structure optimizations were run until forces on ions were smaller than 0.01 eV/Å. For the supported system, a 5-layer Ru slab was used, of which the lowest two Ru layers were held fixed. Dispersion forces were included via the DFT-D2'[35] method.

The cohesive energy E_{COH} is defined in eqn. (1), where E denotes the total energy of the systems. The adhesion energy E_{ADH} of the thin films on Ru(0001) is defined in eqn. (2).

$$E_{COH}(Si_xGe_yO_8) = E(Si_xGe_yO_8) - xE(Si) - yE(Ge) - 4E(O_2) \quad (1)$$

$$E_{ADH}(Si_xGe_yO_8) = E(Si_xGe_yO_8/Ru) - E(Si_xGe_yO_8) - E(Ru) \quad (2)$$

Computational Results

Free-Standing Bilayers

To obtain the structure and the lattice parameters of the different thin films, we optimized the films in the Ru(0001) surface unit cell, which has a lattice parameter of 5.46 Å. Then, we run single point calculations of these optimized structures for different lattice parameters, scaling the internal structure to adapt to the new lattice parameter. This way, we obtained the best lattice parameter. In a final step, we re-optimized the structure at the optimal lattice parameter to obtain the geometries shown in Figure 1.

The Si–Ge compositional space has been sampled by considering mixed oxide model structures with the following ratios: Si(100%), Si(75%)Ge(25%), Si(50%)Ge(50%), Si-(25%)Ge(76%) and Ge(100%). For the $Si_2Ge_2O_8$ stoichiom-

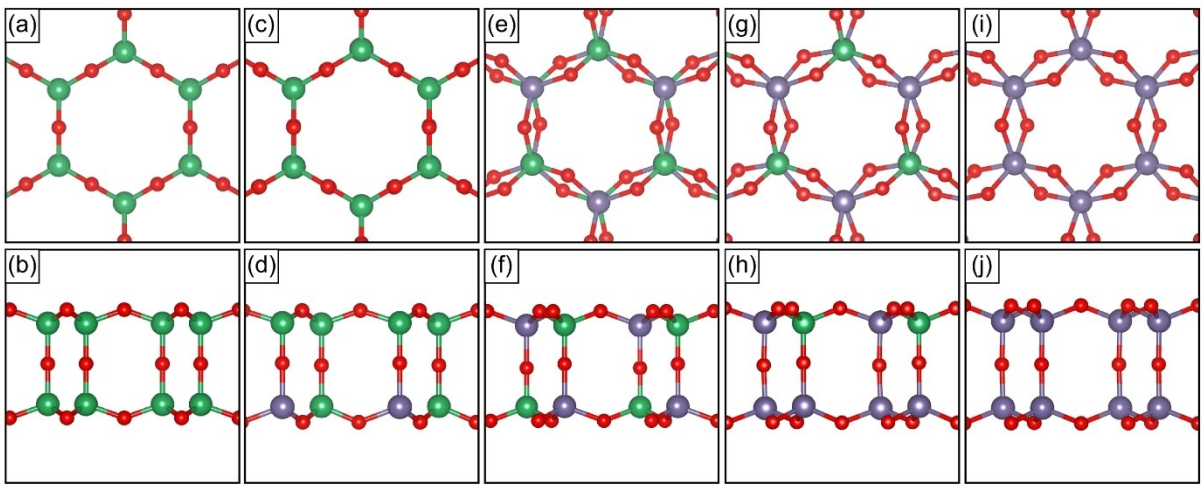

Figure 1. Top view, and side view of (a–b) Si_4O_8, (c,d) $Si_3Ge_1O_8$, (e,f) $Si_2Ge_2O_8$, (g,h) $Si_1Ge_3O_8$, and (i,j) Ge_4O_8. Red: oxygen. Green: silicon. Violet: germanium

etry, there are different possible distributions of the atoms in the bilayer: We denote the first case as "alternating", in which the Ge and Si atoms are alternating in both layers, see Figure 1(e–f). We denote the second case as "segregated". Here, all Ge atoms are in the bottom layer and all Si atoms are in the top layer. In the case of the free-standing bilayers, the alternating structure is slightly more stable than the segregated one (see Table 1). Supported on Ru(0001), the segregated structure becomes more stable due to the stronger interface bond of GeO_2 film as highlighted by the interfacial metal-oxide bonds depicted in Figure 2(g–i).

Ru-Supported Layers

The adhesion energies per MO_2-unit, the distances between the topmost Ru atomic layer and the lowest O atomic layer, and the Bader charges are summarized in Table 2. Note that we considered a $MO_2(1\times1)$ (M=Si, Ge) surface unit cell in all cases which corresponds to a Ru(0001)(2×2) surface unit cell. The resulting system contains 4 M atoms, i.e. $Si_xGe_yO_8$ with $x+y=4$.

Let us compare first the $Si_3Ge_1O_8$ bilayer to the pure silica bilayer. The adhesion energy increases only slightly when one Si atom is replaced by Ge. The Ge atom takes a position in the bottom layer, close to the Ru substrate. The film structure is similar to that of the pure silica bilayer.

For the $Si_2Ge_2O_8$ stoichiometry, we investigated both forms: "alternating" and "segregated". We found that, when supported on Ru(0001), the segregated form with Ge in the bottom layer is more stable than the alternating structure by roughly 1 eV, as deduced from the total energies of the structures considered. The resulting structure for the segregated version is shown in Figure 2(g–i). Interestingly, the upper layer takes a similar geometry as the pure silica bilayer, and the bottom layer takes a similar structure as the germania bilayer. For this structure, the adhesion energy is three times larger as for the pure silica bilayer, Table 2. We detect a charge transfer from the Ru slab to the bilayer, just as in the case of the pure germania bilayer. Thus, when supported on Ru, the Ge atoms should prefer to segregate to the bottom layer of the thin film.

For the $Si_1Ge_3O_8$ stoichiometry, the properties of the pure germania bilayer are basically recovered. However, the adhesion energy is even slightly more negative (by 0.01 eV) than for the pristine germania bilayer, due to the fact that the strain in the bilayer caused by the metal substrate is smaller than for the pure germania bilayer (see Table 1). In all structures, a small charge transfer from the Ru support to the film is observed. The transferred charge is delocalized over the whole film structure.

As a next step, bilayer structures, which are mono- and disubstituted with Ge atoms are supported on 3O-(2×2) Ru(0001). Here the goal is to estimate the chemical shifts in X-ray photoelectron spectra of the O1s ionization, since those may provide qualitative indications on the kind of mixed silica-germania layers are formed. We use PBE functional to perform the calculations. For the comparison between theory and experiment in the last section of the paper it is necessary to also calculate the shifts for the germania monolayer. In calculations of O-1s core level binding energies of the germania monolayer on 3O-(2×2) Ru(0001), we use the structure previously published in Ref. [19], which is shown in Figure 3. In order to identify the O1s ionization site, the oxygen atoms of the systems have been labeled with numbers in side and top view in Figure 3.

Table 1. Cohesive energy (with respect to the gas-phase atoms) of free-standing bilayers E_{COH} (eV) and optimum lattice parameter a (Å).

	E_{COH}	a	Strain (in %) [a]
Si_4O_8	−13.60	5.31	−2.76
$Si_3Ge_1O_8$	−12.34	5.41	−0.92
$Si_2Ge_2O_8$ alternating [b]	−11.21	5.44	−0.37
$Si_2Ge_2O_8$ segregated [b]	−11.10	5.47	+0.17
$Si_1Ge_3O_8$	−10.04	5.45	−0.19
Ge_4O_8	−8.90	5.49	+0.56

[a] Negative and positive values refer to compressive and tensile strain, respectively. [b] "alternating" means Ge and Si alternating in both layers, see Figure 1(e–f), "segregated" means all Ge atoms are in the bottom layer and all Si atoms are in the top layer.

Table 2. Adhesion energy per MO_2-unit E_{ADH} (eV), distance between lowest oxygen layer and uppermost Ru layer, d(Ru–O) (Å), total Bader charge on the Ru slab q_{SUM}(Ru) |e|, average Bader charges on Si, Ge and O atoms, q_{AVG} |e|.

		$E_{ADH}/4$	d(Ru–O)	q_{SUM}(Ru)	q_{AVG}(Si)	q_{AVG}(Ge)	q_{AVG}(O)
Si_4O_8/Ru	top	−0.11	2.65	0.09	3.17	–	−1.60
$Si_3Ge_1O_8$/Ru	top	−0.16	2.50	0.22	3.16	2.24	−1.49
$Si_2Ge_2O_8$/Ru	fcc	−0.35	2.15	0.64	3.17	1.82	−1.33
$Si_1Ge_3O_8$/Ru	fcc	−0.45	2.17	0.60	3.17	1.99	−1.22
Ge_4O_8/Ru	fcc	−0.44	2.17	0.60	–	2.04	−1.09

Israel Journal of Chemistry

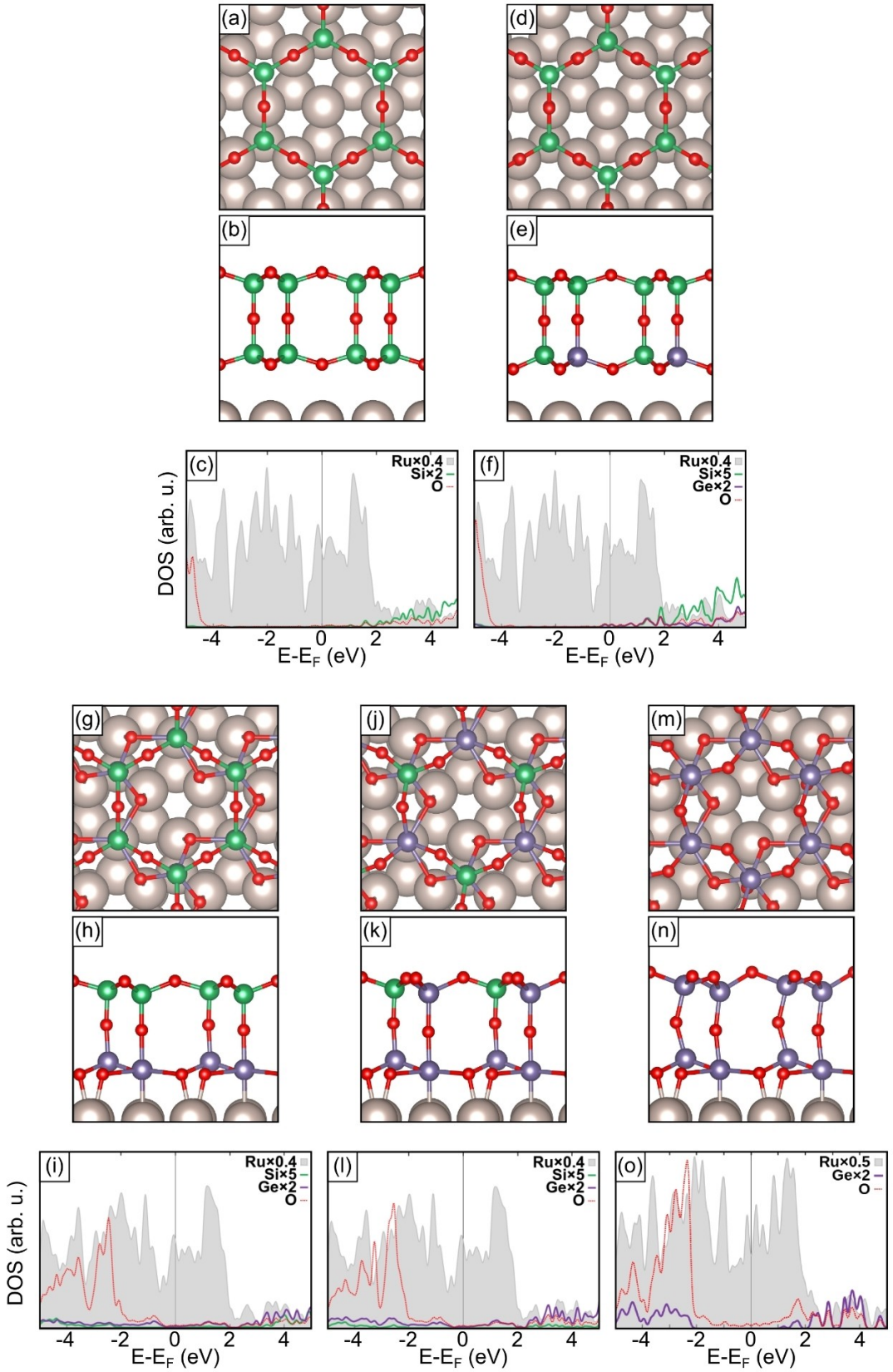

Figure 2. Top view, side view and DOS of (a–c) Si_4O_8/Ru, (d–f) $Si_3Ge_1O_8$/Ru, (g–i) $Si_2Ge_2O_8$/Ru, (j–l) $Si_1Ge_3O_8$/Ru, and (m–o) Ge_4O_8/Ru.

Israel Journal of Chemistry

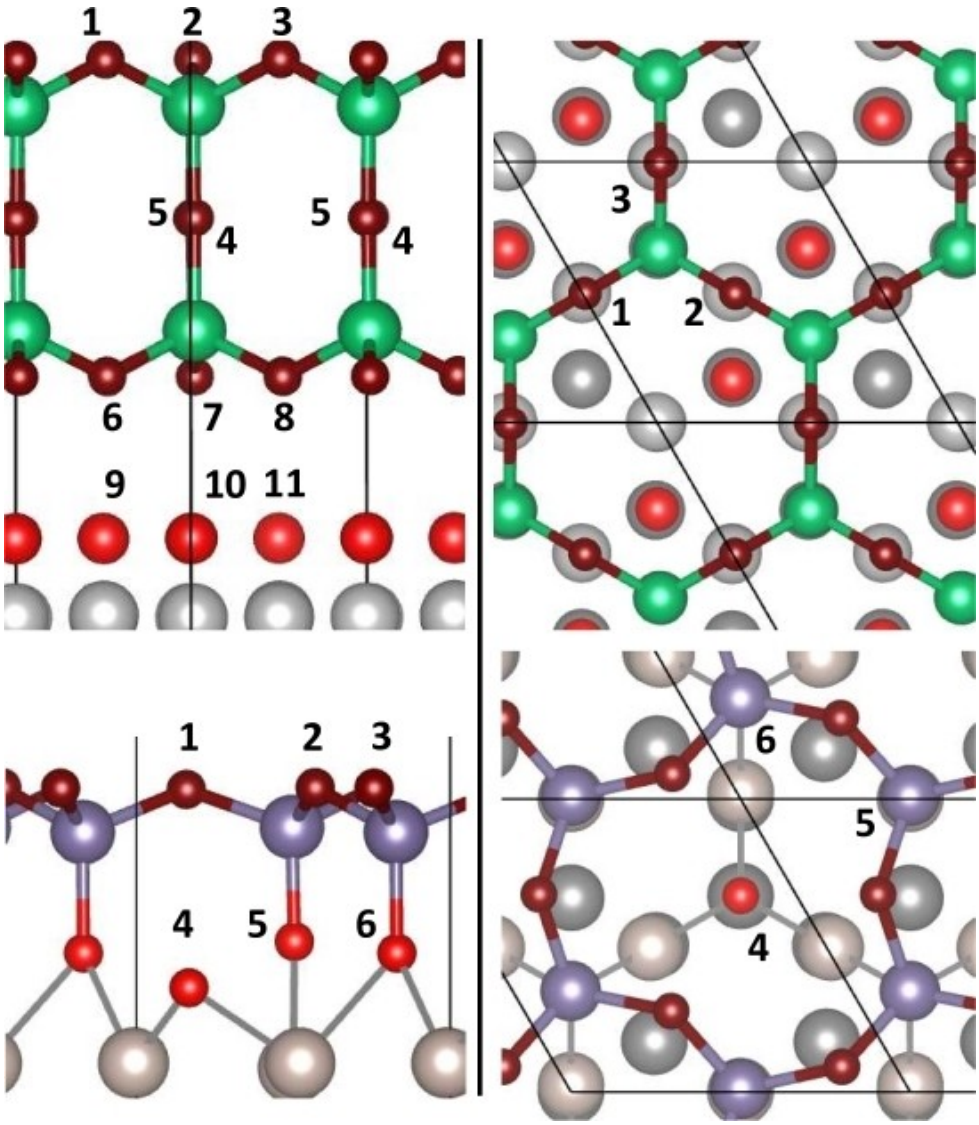

Figure 3. Side and top views on bi- and monolayer systems on 3O-(2×2) Ru(0001). Surface or interface oxygen atoms are red, Ru atoms are grey, oxygen bonded to Si or Ge atoms is dark red, Si atoms are green and Ge atoms are blue. Oxygen atoms are labeled to simplify referring to them (see below).

Intensities of calculated spectra (Figure 7) were weighted such that oxygen atoms in the bilayer add up to approximately one (similar to experiment). In addition, a broadening of 1.0 eV full-width-at-half-maximum Gaussian has been applied. Binding energy shifts obtained using periodic calculations were aligned relative to the absolute BE of 530.69 eV for Ru–O 1s obtained using cluster calculations (Tabel S4) Technical details of periodic calculations have been outlined above. To calculate core orbital excitations, the approach following Slater and Janak[36] as implemented into the VASP code by Köhler and Kresse[37] has been employed. Because total energy differences of electro-neutral and charged systems obtained subject to periodic boundary conditions are difficult to compare,[38] we also accomplished cluster calculations to determine (absolute) binding energies (see SI).

Experimental Results and Discussion: Photoemission (XPS), Low-Energy Electron Emission (LEED,) and Low-Energy Electron Microscopy (LEEM)

Figure 4 shows XPS spectra of relevant core levels of mixed (procedure (i) in Section Experimental details) GeO_2–SiO_2 films (a–c) and of separated (procedure (ii)) GeO_2/SiO_2 films on Ru(0001). For comparison we show in Figure 4(g,h) the XPS spectra of a pure germania monolayer film and in Figure 4(I,j) of a pure silica bilayer film. The maximum intensity of the Ge 3d core level spectrum shown in Figure 4

Israel Journal of Chemistry

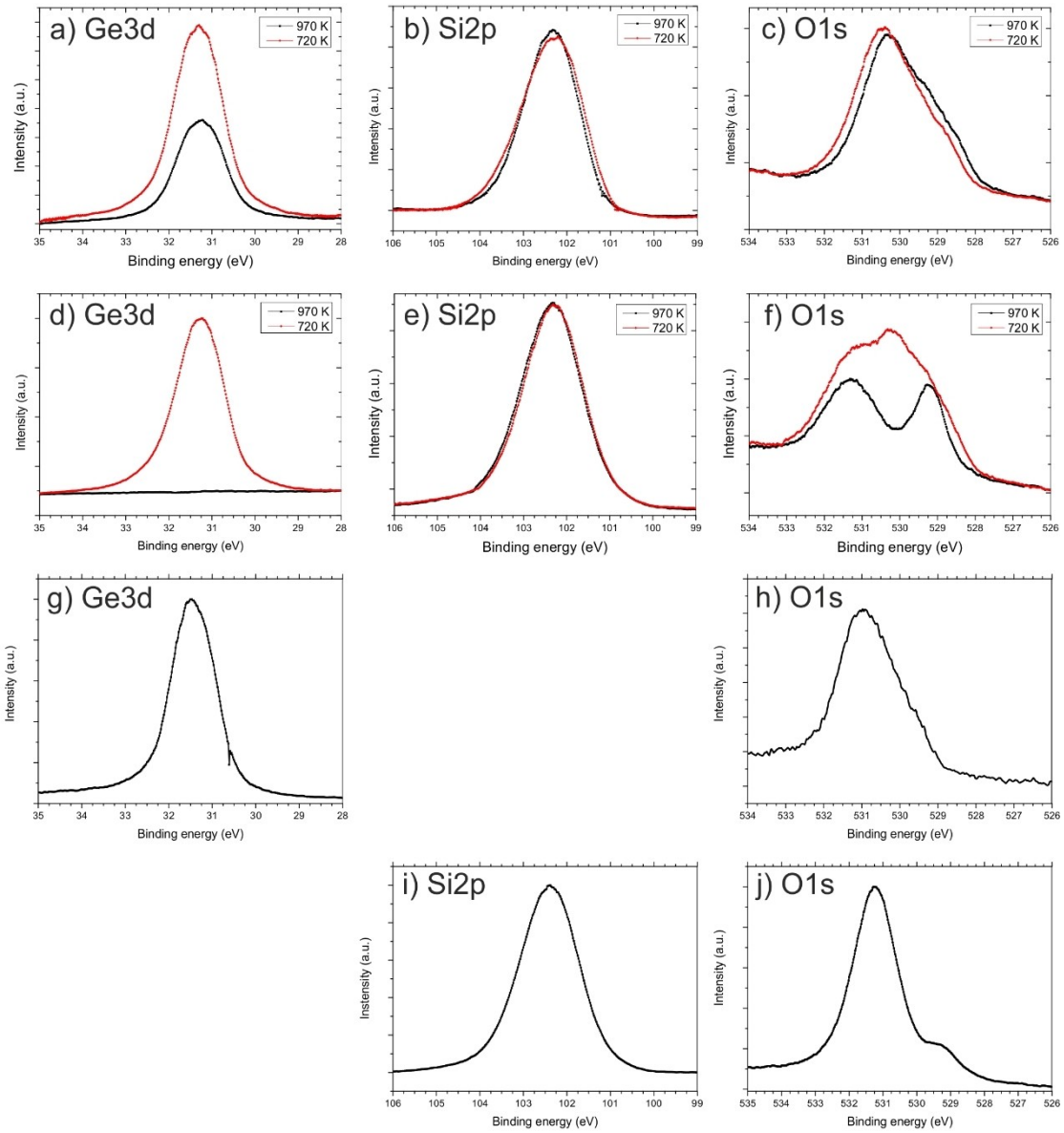

Figure 4. XPS of mixed a Germania-Silica film (a–c) and separated Germania and Silica film (d–f) after annealing to 720 K (red) and 970 K (black) in $1*10^{-6}$ mbar O_2 atmosphere. The used photon energies were 100 eV (Ge3d), 175 eV (Si2p) and 600 eV (O1s); (g,h) show the spectra of a pure germania film(monolayer), and (I,j) those of the pure silica bilayer.

a, (red spectrum) is observed at a binding energy of 31.3 ± 0.1 eV. In comparison, in clean germanium on Ru(0001) the 3d core level is found at a binding energy of about 29.0 ± 0.1 eV for the $Ge3d_{3/2}$ and 28.5 ± 0.1 eV for the $Ge3d_{5/2}$, indicating that Ge in the germania film is completely oxidized after annealing the sample to 720 K in O_2.[29] The intensity of the Ge 3d peak decreases after the second annealing step to 970 K (Figure 4 a, black). This decrease points to desorption of germania that is not bound to the silica. Apart from this intensity decrease no significant core level shift or shape difference between the two spectra is discerned. This observation indicates that the chemical environment of the Ge atoms in the network does not change between the two annealing steps.

In the case where the germanium was deposited on top of an ordered SiO_2 bilayer, for an annealing temperature of 720 K the corresponding Ge 3d core level spectrum shown in Figure 4 d (red) curve is almost identical to the one depicted in Figure 4 a. However, after annealing to 970 K, the Ge 3d spectrum shown in Fig 4 d (black) has vanished, indicating complete desorption of the GeO_2. This observation clearly indicates that for the deposition of germanium on top of an ordered silica bilayer, two separated oxides, silica and germania, have formed without chemical bonds between them.

After annealing the films up to 970 K, the Si2p core level spectra show a binding energy (BE) shift of about 1.0 ± 0.1 eV between the mixed germania-silica film (Figure 4b, $Si2p_{BE}$ = 101.2 ± 0.1 eV) and the separated germania and silica film (Figure 4e, $Si2p_{BE}$ = 102.2 ± 0.1 eV). This observation may reflect the influence of a different environment for Si atoms within a mixed Si–Ge network as compared to the one experienced in the separated films. For the separated silica film, no change in the Si2p core level binding energy between the annealing steps of 720 K and 970 K is observed indicating that the Si atoms in the network are already completely oxidized at 720 K. For the mixed Germania-silica film, a slight broadening of the Si2p core level is observed in the spectra of the Si2p core level of the 970 K annealed film compared to the one at720 K.

We first discuss the comparison between the experimentally observed X-ray photoelectron spectra and the theoretical results, and then turn briefly to the LEEM and LEED results to see whether they are consistent.

Figure 5 compares the O1s XPS spectra of the various samples after fitting them with Lorentzian line shapes. We will concentrate the following discussion of the comparison of experimental and theoretical results on the O1s spectra as they show the most pronounced variation between the samples. A particularly large difference between the mixed germania-silica film and the separated ultrathin oxides is, indeed, reflected by the O1s core level spectra. The O1s core level spectrum of the mixed film shown in Figures 5a and b contains three components, that can be assigned to Si–O, Ru–O, similar to silica on Ru(0001) and additional Ge–O bonds. A detailed analysis of the XPS spectra of silica on Ru(0001) is available in reference.[39] Here, we note that the XPS binding energy for atomic oxygen on Ru(0001) is 529.2 eV[28b] independent of oxygen coverages, varying between one and three oxygen atoms per unit cell. In the mixed germania-silica film, the individual components have a binding energy between 530.4 ± 0.1 eV (Si–O), 529.3 ± 0.1 eV (Ge–O) and 528.5 ± 0.1 eV (Ru–O) - after annealing to 970 K. Slightly higher binding energies of 530.5 ± 0.1 eV (Si–O), 529.6 ± 0.1 eV (Ge–O), and 528.7 ± 0.1 eV (Ru–O) are observed after the first annealing to 720 K. In the separated oxides, the O1s core level also contains three components. After the first annealing (Figure 5b), their binding energies are observed for Si–O at 531.5 ± 0.1 eV, for Ge–O at 530.3 ± 0.1 eV, and for Ru–O at 529.5 ± 0.1 eV. The observed binding energies in the separated oxides (Figure 5c,d) are about 1 eV higher than for the ones in the mixed germania-silica film. After the second annealing to 970 K, the Ge–O component in the O1s core level spectrum is clearly missing. Now the O1s core level spectrum closely resembles the one of a pure silica bilayer indicating that the germania film on top of the ordered silica bilayer had completely desorbed. Moreover, the O1s core level shows a striking difference in peak shape between the mixed and separated oxides. This indicates experimentally the presence of Ge–O, Si–O and Ge–O–Si bonds in the mixed germania-silica film.

On the other hand, the effect of mixing silica and germania on the Si2p and Ge3d core level spectra is weak. With the exception of the binding energy shift, the core level spectra are very similar to the ones of the bare oxides. The influence of silicon on germanium and vice versa in the mixed germania-silica film is negligible. The XPS does not show any evidence

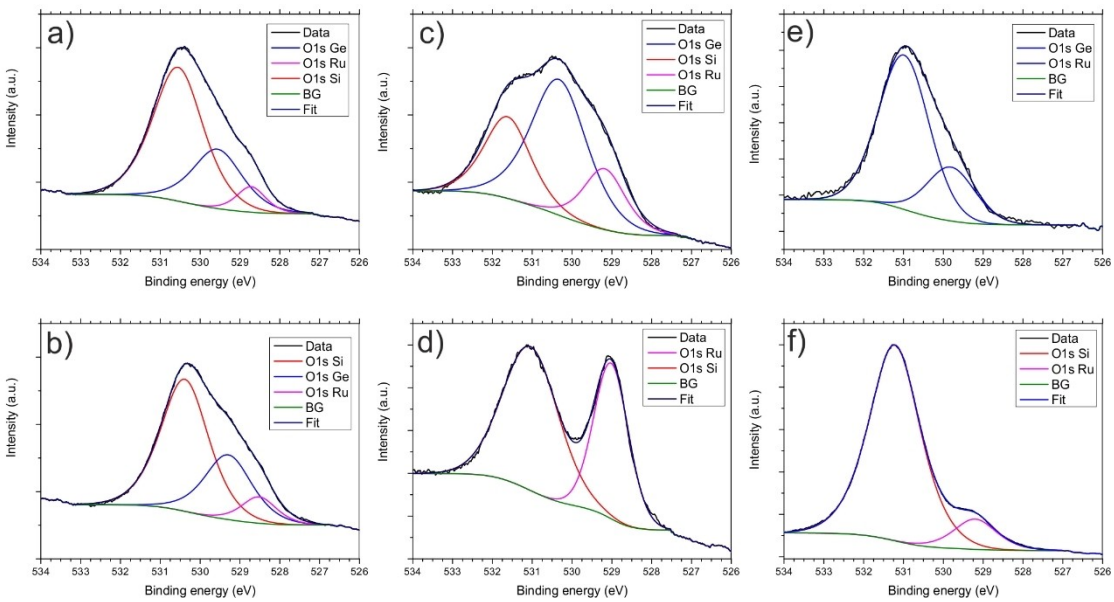

Figure 5. Fitted O1s core level spectra of mixed germania-silica films after annealing to 720 K (a) and 970 K (b), of separated germania and silica film after annealing to 720 K (c), of a silica film after desorption of germania after annealing to 970 K (d), germania ML (e) and silica BL (f). The used photon energy was 600 eV.

for the formation of Si–Ge bonds. If Ge–Si bonds are formed in the mixed oxide, then the Si and Ge core levels should differ from the pure germania monolayer and silica bilayer films by the presence of the Ge–Si bonds.

Figure 6 presents LEED images of the separated oxides (a,b) and the mixed germania-silica oxide (c,d) for different annealing temperatures. All images show a (2×2) pattern that corresponds to a crystalline film.[40] The comparison of the LEED patterns in 5a and b shows that the desorption of germania leads to sharper LEED spots. Desorption from the unbound germania leads to a better ordered film in the remaining silica film. In the case of the mixed germania-silica films (Figure 6 c,d), a higher annealing temperature also leads to sharper LEED spots reflecting a better order of the film. Up to now, we observed only the crystalline (2×2) structure of mixed germania-silica films on Ru(0001). In Figure 5e the LEEM-IV curve for a mixed germania-silica (red) film on Ru(0001) is compared to a pure germania (black) ML on Ru(0001) and a crystalline silica BL (blue) on Ru(0001). The LEEM-IV curve can be used as a fingerprint for the film

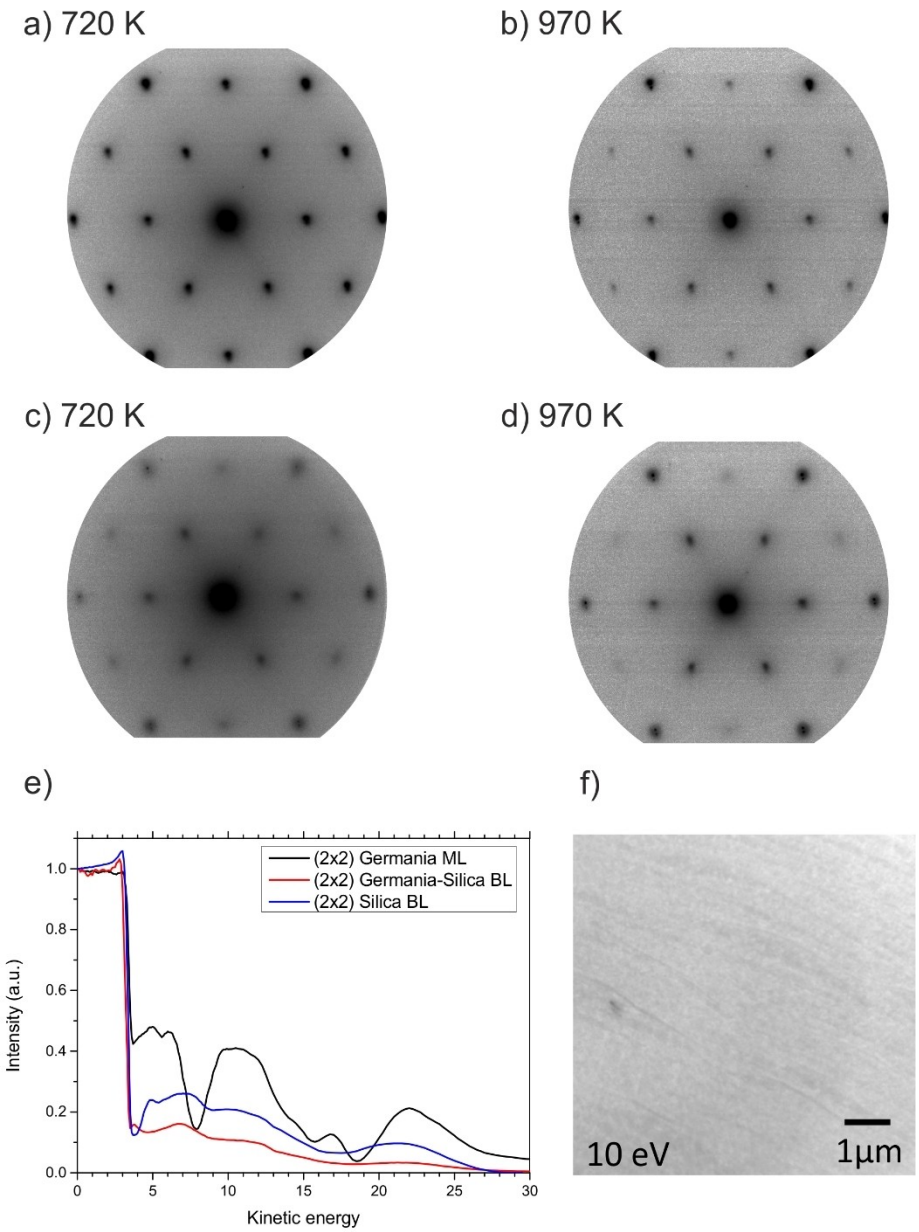

Figure 6. LEED (e-beam energy = 42 eV) of separated germania and silica films after annealing to 720 K (a) and 970 K (b); LEED (42 eV) of mixed germania-silica films after annealing to 720 K (c) and 970 K (d). The LEED patterns were measured at room temperature. LEEM-IV using the (00) LEED-spot intensity of (2×2)-GeO_2 ML, (2×2)-GeO_2–SiO_2 BL and (2×2)-SiO_2 BL (e) and LEEM image of a mixed GeO_2–SiO_2 film after annealing to 970 K at 10 eV e-beam energy (f).

structure. If the kinetic energy of the electron is sufficient to penetrate the sample, there is a strong decrease in the measured reflected intensity, the MEM (mirror electron microscopy) to LEEM transition.[40] The MEM-LEEM transition is a relative measurement of the work function of the sample referred to the work function of the electron gun. For the germania-silica bilayer film (red) the MEM-LEEM transition can be measured at $E_{kin} = 3.25$ eV. The MEM-LEEM transition (this is equivalent to the point in the I/V LEEM curve where the intensity has dropped to half of the maximum value) for the silica BL is observed at 3.39 eV and for the germania ML at 3.55 eV. Adding this value to the electron energy at the electron emitter provides the work function of the system. This indicates that the work function for the mixed silica-germania film is 0.14 eV less than the silica BL which in turn is 0.16 eV less than the germania ML. The work function change is due to three main contributions: (1) an electrostatic "compression" effect, (2) a charge-transfer effect, and (3) the surface relaxation induced by the formation of the interface bond which largely depends on the lattice mismatch between the dielectric film and the metal.[41]

Comparison Between Experiment and Theory and Conclusion

A comparison between experimental XPS spectra and calculated XPS spectra relative to O1s ionization of the oxygen atoms directly bound to the Ru surface is presented in Figure 7.

Figure 7a–e shows calculated O1s photoelectron spectra with respect to surface oxygen atoms (Figure 3, oxygen atoms 9,10 and 11). We need to realize, that the experimental spectrum of the pure GeO_2-film represents a monolayer film, which leads to a bonding situation different from all other cases. This implies specific chemical shifts to lower binding energy, connected with Ge–O-metal bonds. Those do not exist in bilayer films. The deconvolution of the experimental spectrum (g) reveals, in this special case, the shift of the Ge–O–Ru bond to lowest binding energy, due to the presence of the larger negative charge on the oxygen atom participating in this bond as compared to surface oxygen, which is the reference point (see Table S5). This renders a direct comparison difficult, but the trends in the spectral shapes are reproduced. Note that intensities were not calculated from first principles, but just weighted according to the content per unit cell, i.e., three O atoms on the Ru surface (Figure 3) and eight O atoms in the bilayer. To calculate those spectra, we use the possibility to include in periodic DFT calculations the influence of the substrate on binding energy (BE) shifts via utilization of repeated slab models (see previous section). Nonetheless, in order to disentangle initial from final state contributions to BE shifts upon creation of a positively charged core hole, O1s orbital energies or eigenvalues for electroneutral as well charged models need to be compared. However, this is difficult in periodic DFT since the electrostatic energy of systems described with a charged unit cell diverges. As a remedy, inclusion of a charge compensating (homogeneous) background has been introduced by Makov and Payne.[34] Approaches devised to align the average electrostatic potential to compute for instance formation energies of charged defects via periodic DFT are related to the above-described issue.[42] For comparison of absolute BEs in the present work, we circumvent these issues and thus accomplished Hartree-Fock calculations using finite cluster models together with open-boundary conditions. These calculations use as a reference the vanishing potential (energy) of an infinitely separated (photo-) electron, and therefore the electrostatic potential as well as the orbital energies are well defined.[43]

Turning now to a discussion of numerical results, Tables S1 - S3 compile initial state approximation (ISA) and final state approximation (FSA) results, where the latter include orbital relaxation effects due to the positively charged O1s core hole upon photoionization. Table S1 shows results for the pure SiO_2 and GeO_2 bilayers and Table S2 summarizes results for bilayers of SiO_2 with one Si replaced by Ge (monosubstituted SiO_2, Table S2). Table S3 shows corresponding results for disubstituted SiO_2 bilayers. On passing, we mention that within DFT, the interpretation of (negative) eigenvalues as BEs is not theoretically justified as in (closed-shell) Hartree-Fock theory. The latter is known as Koopmans' theorem. For instance, estimating the relaxation energy or core-hole screening effects for Ru–O 1s, i.e., O_{surf}, 9, 10, 11 in Figure 3 by taking the difference between ISA and FSA results, one obtains ca. 32.2 eV for surface oxygen ions and a much larger value of ca. 35–36 eV for 1 s orbitals in the bridging O species in the bilayer. This is counterintuitive, as the core-hole screening in the surface is supposed to be much more efficient, and thus relaxation effects are expected to be largest for Ru–O1s. This apparently wrong result can be understood considering the discussion above. In contrast, cluster results for a relatively small $Ru_{19}O$ cluster and H-saturated $Si_2O_7H_6$ and $Ge_2O_7H_6$ clusters (Table S4) yield a relaxation energy for Ru–O1s of 25.5 eV being 3–4 eV larger than corresponding contributions to BEs in Si/Ge–O1s. Apparently, results for the $SiGeO_7H_6$ cluster, representing O1s in the mixed oxide phase, are erroneous, supposedly due to the restricted-open-shell HF approach, which neglects electronic correlation effects. Corresponding results obtained using DFT appear to treat models for pure and mixed phases on equal footing. Although, it is well understood that BEs obtained using either HF or DFT may suffer from substantial errors, we adjusted the energy scale in Figures 7a)–e) such that Ru–O1s BEs are equal to the final state HF cluster result, i.e., 530.69 eV.

To summarize the comparison between theory and experiment concerning the O 1s core level binding energy shifts, the calculated binding energies show the same trend as observed in the experiment; starting from their position in silica and germania, they shift towards smaller binding energies in the mixed silica-germania films.

Israel Journal of Chemistry

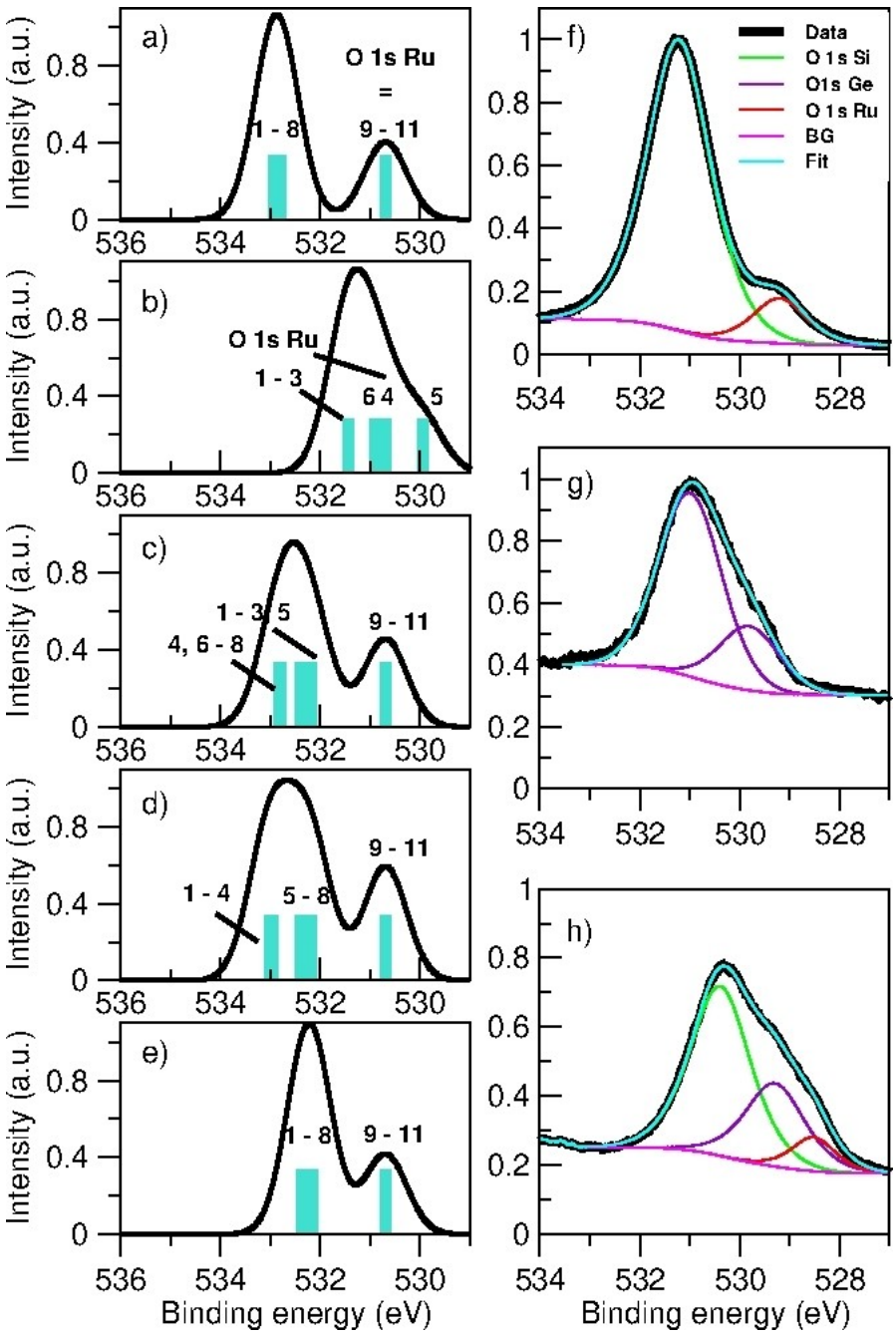

Figure 7. Comparison of calculated (a–e) and observed (f–h) O1s binding energies (eV) for pure and mixed silica and germania systems. The experimental spectra in (f–h) are taken from Figure 5 to allow for direct comparison. To compare, pure SiO_2 bilayers are shown in a) and f); pure Germania monolayer phases are shown in b) and g); monosubstituted SiO_2 with one Ge atom in the upper and lower layer are shown in c) and d), respectively. Results for the disubstituted (2 Ge atoms) SiO_2 bilayer are shown in e). Labels shown in calculated spectra refer to ionization sites displayed in Figure 3, whereas observed results give absolute binding energies. The observed spectra for the mixed silica/germania are shown in h).

Note that theoretical and experimental results on bilayer systems, shown in Figure 7, agree on the fact that the O_{surf} 1s states "feel" the electronic nature of the bilayer. Therefore, corresponding BEs shift slightly depend on the composition of the bilayer and the actual site of Si-substituting Ge atoms (i. e., near surface in the bottom (mono-)layer or more distant in the top-layer).

The LEEM-IV curve of the pure germania ML (black) is clearly different from the LEEM-IV curves of germania-silica BL (red) and pure silica BL (blue) (see Figure 5). The LEEM-

IV curve of the germania ML shows a double peak feature between 5 eV and 7 eV and a prominent dip at 8 eV. On the other hand, the LEEM-IV curve of the mixed germania-silica film shows features which are similar to the one of the pure silica BL but at a lower intensity. This behavior indicates that the structure of the mixed silica-germania film is mainly dominated by the silica BL-structure. Due to defects induced by the Ge atoms, the intensity of the IV curve for the mixed silica-germania BL film decreases with respect to the one for the pure silica BL film. This effect most probably causes also the slightly blurred LEED spots observed in Figure 5 d.

A typical LEEM image of a mixed germania-silica film is presented in Figure 5f. The atomic steps and step bunches of the Ru(0001) substrate appear as dark lines. The atomic steps proceed from the top left to the bottom right in the LEEM image. The LEEM image shows a homogeneous germania-silica film. Within the resolving power of the LEEM, no contrast differences can be observed that indicate phase separation of germania-rich and germania-poor regions.

To summarize the conclusions drawn from the present study, we note that the combined analysis of x-ray photoelectron spectra, LEED and LEEM data allows us to determine whether or not a mixed silica-germania film is formed, and thus delivers important insight for future studies, when those films are used as membranes or as models to study chemistry in confined space, as reported for pure silica films recently. The higher structural flexibility of the O–Ge–O unit in comparison to O–Si–O may allow to control the migration of molecules of different size through the film.[10,44]

Acknowledgements

We thank the BESSY II crew for their support and the Helmholtz-Center Berlin for Materials and Energy (HZB) for the allocation of beamtime. We acknowledge the financial support by the Federal German Ministry of Education and Science (BMBF) under Contract no. 05KS4WWB/4. The authors thank Dietrich Menzel, Markus Heyde, Thomas Schmidt and all members of Thomas Schmidt's group especially Mauricio Prieto for helpful discussions. JP thanks Professor Joachim Sauer for permission to use some of his computational facilities. Open Access funding enabled and organized by Projekt DEAL.

Data Availability Statement

The data that support the findings of this study are available from the corresponding author upon reasonable request.

References

[1] K. S. Novoselov, A. Mishchenko, A. Carvalho, A. H. Castro Neto, *Science* **2016**, *353*, aac9439.
[2] G. Barcaro, A. Fortunelli, *Phys. Chem. Chem. Phys.* **2019**, *21*, 11510–11536.
[3] a) T. Yang, T. T. Song, M. Callsen, J. Zhou, J. W. Chai, Y. P. Feng, S. J. Wang, M. Yang, *Adv. Mater. Interfaces* **2019**, *6*, 1801160; b) S. Ida, T. Ishihara, *J. Phys. Chem. Lett.* **2014**, *5*, 2533–2542; c) O. J. Clark, O. Dowinton, M. S. Bahramy, J. Sánchez-Barriga, *Nat. Commun.* **2022**, *13*, 4147.
[4] N. F. Richter, H. Ronneburg, P. M. Clawin, N. Subat, F. E. Feiten, J. Pal, E. Emmez, S. Shaikhutdinov, H. Kuhlenbeck, T. Risse, H.-J. Freund, *J. Phys. Chem. C* **2022**, *126*, 7956–7964.
[5] J. Sauer, H.-J. Freund, *Catal. Lett.* **2015**, *145*, 109–125.
[6] F. Liebau, *Structural Chemistry of Silicates*, **Springer**, Berlin Heidelberg, **2012**, p.
[7] D. Kuhness, H. J. Yang, H. W. Klemm, M. Prieto, G. Peschel, A. Fuhrich, D. Menzel, T. Schmidt, X. Yu, S. Shaikhutdinov, A. Lewandowski, M. Heyde, A. Kelemen, R. Włodarczyk, D. Usvyat, M. Schütz, J. Sauer, H.-J. Freund, *J. Am. Chem. Soc.* **2018**, *140*, 6164–6168.
[8] W. H. Zachariasen, *J. Am. Chem. Soc.* **1932**, *54*, 3841–3851.
[9] L. Lichtenstein, M. Heyde, H.-J. Freund, *J. Phys. Chem. C* **2012**, *116*, 20426–20432.
[10] J.-Q. Zhong, H.-J. Freund, *Chem. Rev.* **2022**, *122*, 11172–11246.
[11] G. S. Hutchings, X. Shen, C. Zhou, P. Dementyev, D. Naberezhnyi, I. Ennen, A. Hütten, N. Doudin, J. H. Hsu, Z. S. Fishman, U. D. Schwarz, S. Hu, E. I. Altman, *2D Mater.* **2022**, *9*, 021003.
[12] A. L. Lewandowski, S. Tosoni, L. Gura, P. Schlexer, P. Marschalik, W.-D. Schneider, M. Heyde, G. Pacchioni, H.-J. Freund, *Angew. Chem. Int. Ed.* **2019**, *58*, 10903–10908; *Angew. Chem.* **2019**, *131*, 11019–11024.
[13] A. L. Lewandowski, S. Tosoni, L. Gura, Z. Yang, A. Fuhrich, M. J. Prieto, T. Schmidt, D. Usvyat, W.-D. Schneider, M. Heyde, G. Pacchioni, H.-J. Freund, *Chem. Eur. J.* **2021**, *27*, 1870–1885.
[14] N. Doudin, K. Saritas, M. Li, I. Ennen, J. A. Boscoboinik, P. Dementyev, A. Hütten, S. Ismail-Beigi, E. I. Altman, *ACS Materials Lett.* **2022**, *4*, 1660–1667.
[15] U. K. Thiele, *Int. J. Polym. Mater.* **2001**, *50*, 387–394.
[16] N. Jiang, J. Qiu, A. L. Gaeta, J. Silcox, *Appl. Phys. Lett.* **2002**, *80*, 2005–2007.
[17] J. D. Esper, F. Maußner, S. Romeis, Y. Zhuo, M. K. S. Barr, T. Yokosawa, E. Spiecker, J. Bachmann, W. Peukert, *Energy Technol.* **2022**, *10*, 2200072.
[18] V. A. Volodin, G. N. Kamaev, V. A. Gritsenko, A. A. Gismatulin, A. Chin, M. Vergnat, *Appl. Phys. Lett.* **2019**, *114*, 233104.
[19] A. L. Lewandowski, P. Schlexer, C. Büchner, E. M. Davis, H. Burrall, K. M. Burson, W.-D. Schneider, M. Heyde, G. Pacchioni, H.-J. Freund, *Phys. Rev. B* **2018**, *97*, 115406.
[20] A. L. Lewandowski, F. Stavale, S. Tosoni, W. D. Schneider, M. Heyde, G. Pacchioni, H. J. Freund, *Phys. Rev. B* **2019**, *100*, 241403.
[21] L. Lichtenstein, C. Büchner, B. Yang, S. Shaikhutdinov, M. Heyde, M. Sierka, R. Włodarczyk, J. Sauer, H.-J. Freund, *Angew. Chem. Int. Ed.* **2012**, *51*, 404–407; *Angew. Chem.* **2012**, *124*, 416–420.
[22] a) J. G. Bendoraitis, A. W. Chester, F. G. Dwyer, W. E. Garwood, in: *Pore Size and Shape Effects in Zeolite Catalysis, Vol. 28* Eds.: Y. Murakami, A. Iijima, J. W. Ward), Elsevier, **1986**, pp. 669–675; b) N. Kasian, E. Verheyen, G. Vanbutsele, K. Houthoofd, T. I. Koranyi, J. A. Martens, C. E. A. Kirschhock, *Microporous Mesoporous Mater.* **2013**, *166*, 153–160.

[23] A. Corma, M. J. Díaz-Cabañas, J. Martínez-Triguero, F. Rey, J. Rius, *Nature* **2002**, *418*, 514–517.
[24] a) T. Schmidt, H. Marchetto, P. L. Lévesque, U. Groh, F. Maier, D. Preikszas, P. Hartel, R. Spehr, G. Lilienkamp, W. Engel, R. Fink, E. D. Bauer, H. Rose, E. Umbach, H. J. Freund, *Ultramicroscopy* **2010**, *110*, 1358–1361; b) T. Schmidt, A. Sala, H. Marchetto, E. Umbach, H. J. Freund, *Ultramicroscopy* **2013**, *126*, 23–32.
[25] T. E. Madey, H. Albert Engelhardt, D. Menzel, *Surf. Sci.* **1975**, *48*, 304–328.
[26] C. N. R. Rao, P. V. Kamath, S. Yashonath, *Chem. Phys. Lett.* **1982**, *88*, 13–16.
[27] a) K. L. Kostov, M. Gsell, P. Jakob, T. Moritz, W. Widdra, D. Menzel, *Surf. Sci.* **1997**, *394*, L138–L144; b) M. Gsell, M. Stichler, P. Jakob, D. Menzel, *Isr. J. Chem.* **1998**, *38*, 339–348.
[28] a) H. W. Klemm in, *Formation and properties of ultrathin silicon dioxide films on Ru(0001): an in-situ spectro-microscopy study.*, *Vol. Dr. Ing.* Technische Universität Berlin, **2018**; b) H. W. Klemm, M. J. Prieto, G. Peschel, A. Fuhrich, E. Madej, F. Xiong, D. Menzel, T. Schmidt, H.-J. Freund, *J. Phys. Chem. C* **2019**, *123*, 8228–8243.
[29] A. Fuhrich, in *Ultra-thin Germania and Germania-Silica films: Growth*, *structure and reactivity*, *Vol. PhD Thesis* Freie Universität Berlin, Berlin, **2019**.
[30] H. W. Klemm, G. Peschel, E. Madej, A. Fuhrich, M. Timm, D. Menzel, T. Schmidt, H. J. Freund, *Surf. Sci.* **2016**, *643*, 45–51.
[31] a) G. Kresse, J. Furthmüller, *Comput. Mater. Sci.* **1996**, *6*, 15–50; b) G. Kresse, J. Furthmüller, *Phys. Rev. B* **1996**, *54*, 11169.
[32] J. P. Perdew, K. Burke, M. Ernzerhof, *Phys. Rev. Lett.* **1996**, *77*, 3865.
[33] H. J. Monkhorst, J. D. Pack, *Phys. Rev. B* **1976**, *13*, 5188–5192.
[34] G. Makov, M. C. Payne, *Phys. Rev. B* **1995**, *51*, 4014–4022.
[35] a) L. Gura, S. Tosoni, A. L. Lewandowski, P. Marschalik, Z. Yang, W.-D. Schneider, M. Heyde, G. Pacchioni, H.-J. Freund, *Phys. Rev. Mater.* **2021**, *5*, L071001; b) S. Tosoni, J. Sauer, *Phys. Chem. Chem. Phys.* **2010**, *12*, 14330–14340.
[36] a) J. C. Slater, in *Statistical Exchange-Correlation in the Self-Consistent Field, Vol. 6* (Ed. P.-O. Löwdin), Academic Press, **1972**, pp. 1–92; b) J. F. Janak, *Phys. Rev. B* **1978**, *18*, 7165–7168.
[37] L. Köhler, G. Kresse, *Phys. Rev. B* **2004**, *70*, 165405.
[38] C. Freysoldt, B. Grabowski, T. Hickel, J. Neugebauer, G. Kresse, A. Janotti, C. G. Van de Walle, *Rev. Mod. Phys.* **2014**, *86*, 253–305.
[39] R. Włodarczyk, M. Sierka, J. Sauer, D. Löffler, J. J. Uhlrich, X. Yu, B. Yang, I. M. N. Groot, S. Shaikhutdinov, H. J. Freund, *Phys. Rev. B* **2012**, *85*, 085403.
[40] a) E. Bauer, *Rep. Progr. Phys* **1994**, *57*, 895–938; b) G. F. Nataf, P. Grysan, M. Guennou, J. Kreisel, D. Martinotti, C. L. Rountree, C. Mathieu, N. Barrett, *Sci. Rep.* **2016**, *6*, 33098.
[41] S. Prada, U. Martinez, G. Pacchioni, *Phys. Rev. B* **2008**, *78*, 235423.
[42] F. Gallino, G. Pacchioni, C. D. Valentin, *J. Chem. Phys.* **2010**, *133*, 144512.
[43] L. Kleinman, *Phys. Rev. B* **1981**, *24*, 7412–7414.
[44] a) M. J. Prieto, H. W. Klemm, F. Xiong, D. M. Gottlob, D. Menzel, T. Schmidt, H.-J. Freund, *Angew. Chem. Int. Ed.* **2018**, *57*, 8749–8753; *Angew. Chem.* **2018**, *130*, 8885–8889; b) M. J. Prieto, T. Mullan, M. Schlutow, D. M. Gottlob, L. C. Tănase, D. Menzel, J. Sauer, D. Usvyat, T. Schmidt, H.-J. Freund, *J. Am. Chem. Soc.* **2021**, *143*, 8780–8790.

Manuscript received: January 16, 2023
Revised manuscript received: February 2, 2023
Version of record online: February 21, 2023